

Histopathology Slide Indexing and Search: Are We There Yet?

Helen H. Shang, MD, MS^{*,1,3} Mohammad Sadegh Nasr^{*,3,4} Jai Prakash Veerla^{3,4}
 Parisa Boodaghi Malidarreh^{3,4} MD Jillur Rahman Saurav^{3,4} Amir Hajighasemi^{3,4}
 Manfred Huber³ Chace Moleta, MD² Jitin Makker, MD² Jacob M. Lubner,
 PhD^{†,3,4,5,6}

¹*Department of Internal Medicine, Ronald Reagan University of California Los Angeles Medical Center*

²*Department of Pathology & Laboratory Medicine, Ronald Reagan University of California Los Angeles Medical Center*

³*Department of Computer Science and Engineering, The University of Texas at Arlington*

⁴*Multi-Interprofessional Center for Health Informatics, The University of Texas at Arlington*

⁵*Department of Bioengineering, The University of Texas at Arlington*

⁶*Department of Biology, The University of Texas at Arlington*

Abstract

The search and retrieval of digital histopathology slides is an important task that has yet to be solved. In this case study, we investigate the clinical readiness of three state-of-the-art histopathology slide search engines, Yottixel, SISH, and RetCCL, on three patients with solid tumors. We provide a qualitative assessment of each model’s performance in providing retrieval results that are reliable and useful to pathologists. We found that all three image search engines fail to produce consistently reliable results and have difficulties in capturing granular and subtle features of malignancy, limiting their diagnostic accuracy. Based on our findings, we also propose a minimal set of requirements to further advance the development of accurate and reliable histopathology image search engines for successful clinical adoption.

1 Introduction

As histopathology slides become increasingly digitized, the process of manually searching and retrieving slides has become increasingly more time-consuming for pathologists (). Recently, there has been growing interest in the development of automated search and retrieval systems for digital histopathology slides (), which can help pathologists identify similar cases in developing a broader differential diagnosis. There has been widespread disagreements between the groups who have created these methods (Sikaroudi et al., 2023). These systems leverage advances in artificial intelligence and machine learning to analyze large volumes of slides efficiently and accurately.

The exploration of medical image databases predominantly relies on content-based image retrieval (CBIR) (). CBIR systems initially transform images into a feature-based database accompanied by corresponding indices. Subsequently, by utilizing a similarity metric, the retrieval process simplifies into a k-nearest neighbors problem. Extracting features from extensive whole slide images (WSI) is typically achieved through either the sub-setting method, which focuses on a small section of a large pathology image to significantly reduce processing time, or the tiling method, which segments images into manageable patches (i.e., tiles) for intra-patch processing ().

Among the recent end-to-end systems proposed for histopathology image search, Yottixel (Kalra, Tizhoosh, Choi, et al., 2020), SISH (Chen et al., 2022), and RetCCL (Wang et al., 2023) have emerged as influential contenders, showcasing promising outcomes. Yottixel pioneered the processing of large-scale WSIs by introducing the concept of mosaics. Instead of extracting features from the entire WSI, Yottixel’s approach involves extracting features from mosaic tiles using a DenseNet-based feature extractor. Additionally, Yottixel incorporates the notion of barcoding () to facilitate expedited retrieval

*These authors contributed equally to this work.

†Corresponding author. Email: jacob.lubner@uta.edu

by binarizing the extracted features. Similarly, SISH adopts a similar framework to Yottixel but incorporates an additional VQ-VAE-based (Oord et al., 2018) feature extractor. SISH also introduces advanced VEB tree-based (van Emde Boas, 1977) indexing and ranking algorithms to enhance the retrieval phase’s time complexity. In contrast, RetCCL employs the mosaic concept as well, but uniquely converts WSIs to mosaics after extracting features from tiled WSIs. Moreover, RetCCL introduces an effective contrastive-based feature extractor to improve feature quality.

The introduction of successive systems claiming to have achieved state-of-the-art performance in the search and retrieval of histopathology slides, often supported by statistical metrics demonstrating agreement with trained pathologists’ judgments, raises the fundamental question of whether this problem has been satisfactorily addressed. Specifically, it prompts an inquiry into the readiness of these systems for deployment in clinical settings, where they can provide genuinely valuable information to pathologists, especially in challenging cases that even the most experienced pathologists struggle to reach a unanimous consensus. Given that the end users of these models are pathologists, their ability to extract pertinent and meaningful information from these systems becomes crucial in alleviating their workload burdens, regardless of the systems’ technical sophistication.

In this case study, we evaluate these models on three previously unseen patient cases from our health system. Our objective is not to provide a quantitative statistical analysis of these models’ performance, as the respective authors have already accomplished that, but to offer a qualitative assessment of the usefulness of these models in the clinical setting. Our test cases encompass less controversial diagnoses, enabling a qualitative evaluation of each model’s performance under clinical conditions. To ensure fairness, we constructed each model’s database using a fixed number of slides from The Cancer Genome Atlas (TCGA) (Weinstein et al., 2013), while employing the same feature extractors as published by the original authors.

In the subsequent sections, we provide an overview of our methods and approach towards implementation (Section 2). We then report our qualitative analysis of each model’s performance on three patient cases (Section 3). Finally, we discuss the current state of histopathology slide search engines and propose a set of minimal requirements for real-world deployment (Section 4).

2 Methods

2.1 Search Engines

Search engines commonly comprise two fundamental components: indexing and database generation, as well as ranking and retrieval. Given the large-scale nature of the images involved in this study, feature extraction becomes imperative for effective indexing. In terms of ranking, a suitable similarity measure is crucial, followed by post-processing steps to ensure result quality. In the supplementary methods section, we provide an overview of the feature extraction techniques, database indexing approaches, employed similarity measures, and result ranking methodologies utilized by the three primary methods under investigation (Fig. 1). Please be advised that all the hyper-parameters employed here are the parameters recommended by the authors of the models. We additionally share our code that we used to re-implement methods that were not made available by the authors.

To summarize, The **Yottixel** method creates a mosaic of patches from whole slide images (WSIs), applies a feature extractor, KimiaNet (Riasatian et al., 2021), and generates binary codes, or barcodes, from the extracted features. These barcodes represent each WSI, form a database, and enable the retrieval of related slides or patches based on the median of the minimum Hamming distances (Hamming, 1950).

The **SISH** method also generates a mosaic and uses DenseNet for feature extraction similar to Yottixel, but it further employs a pretrained VQ-VAE for index creation. Querying in SISH involves converting a slide into a mosaic, generating indices and features, and utilizing the "guided VEB search" algorithm to retrieve top slides based on Hamming distance.

RetCCL takes inspiration from both Yottixel and SISH but applies a unique approach by obtaining contrastive-based feature vectors for each patch within the segmented foreground tiles. The method employs a clustering-guided contrastive learning method with two InfoNCE losses to capture irregular regions in patches, which is particularly important given the prevalence of normal cells in WSIs (Oord et al., 2019).

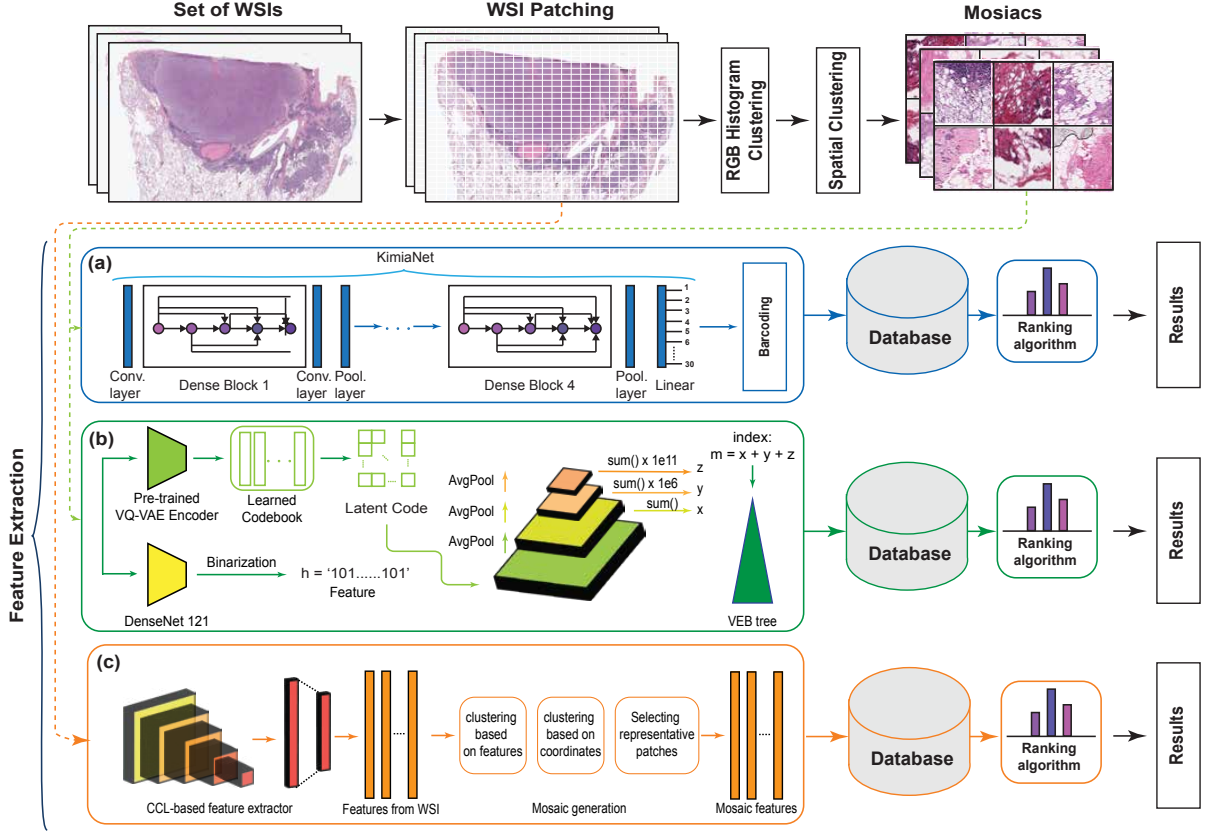


Figure 1: A summary of indexing and retrieval methods of Yottixel (Kalra, Tizhoosh, Choi, et al., 2020) plus KimiaNet (Riasatian et al., 2021), SISH (Chen et al., 2022), and RetCCL (Wang et al., 2023). (a) Feature extractor for Yottixel, (b) for SISH, and (c) for RetCCL.

2.2 Database Slides

To ensure a fair comparison among all models, it was necessary to have consistent slides in the databases of each model. We constructed the database using slides available in TCGA (Weinstein et al., 2013). Given our focus on lung, brain, and liver as primary sites for testing (see Section 2.3), it was essential to include slides from these sites in the databases. Additionally, to introduce a challenging aspect, slides from breast and colon were added to ensure that site retrieval experiments were not trivial. For each site, we randomly selected between 50 to 75 slides from subtypes containing at least 75 slides. The varying number of slides aimed to introduce class imbalance, mirroring real-world scenarios where some subtypes have more samples than others. Importantly, none of the slides in the database shared the same patient ID. The resulting database comprised 508 slides from 5 different sites and 8 different subtypes (Table 1).

It is worth noting that in each experiment, we utilized the pre-trained feature extractors provided by the respective authors. These feature extractors were trained on different datasets of varying sizes. The relatively small size of our database does not affect the performance of these models, as the only aspect influenced by data size is the feature extractor. As long as we have samples of the same class as the query within the database, a correctly functioning model should be capable of retrieving them.

Due to preprocessing criteria, we were not able to include 6 slides for Yottixel and 1 slide for SISH in the database. These slides are listed in Supplementary Table 1.

2.3 Tissue and Subtype Retrieval Experiments

We define “Tissue” as the tissue of cancer origin and “Subtype” as the final diagnosis, which is specific to the tissue type. All slides were sourced from real clinical cases at our institution to best approximate real-world scenarios. Team members who were responsible for algorithmic implementation were blinded from the ground truth to reduce the likelihood of bias.

Table 1: Summary of database used for comparison experiments .Abbreviations are based on (Kalra, Tizhoosh, Shah, et al., 2020).

Primary Site	Project Name (Subtype)	Abbr.	Num. Slides	Num. Selected Slides
Brain	Glioblastoma Multiforme	GBM	2040	61
	Brain Lower Grade Glioma	LGG	1543	69
	Lymphoid Neasm Diffuse Large B-cell Lymphoma	DLBC	4	0
Breast	Breast Invasive Carcinoma	BRCA	2704	72
	Lymphoid Neasm Diffuse Large B-cell Lymphoma	DLBC	2	0
Bronchus and lung	Lung Adenocarcinoma	LUAD	1359	68
	Lung Squamous Cell Carcinoma	LUSC	1265	57
	Mesothelioma	MESO	2	0
Colon	Colon Adenocarcinoma	COAD	1307	59
	Rectum Adenocarcinoma	READ	18	0
	Lymphoid Neasm Diffuse Large B-cell Lymphoma	DLBC	6	0
	Sarcoma	SARC	4	0
Liver and intrahepatic bile ducts	Liver Hepatocellular Carcinoma	LIHC	778	72
	Cholangiocarcinoma	CHOL	80	50

For subtype experiments, we limited the search database to the slides with the same tissue type as the query. This was also true for patch retrieval experiments. A summary of the test slides used for these experiments is provided in Table 2.

Table 2: Summary of test slides and corresponding diagnoses used for comparison experiments.

Slide	Subtype	Tissue	Source
Slide 1	Lung adenocarcinoma	Lung	Surgical resection
Slide 2	Astrocytoma/Low grade glioma	Brain	Surgical resection
Slide 3	Hepatocellular carcinoma	Liver	FNA Biopsy

3 Results

Detailed results are included in the supplement, and a concise summary is provided here.

3.1 Lung Adenocarcinoma Slide Retrieval

The highest performing model for retrieving Lung Adenocarcinoma (LUAD) slides using subtype search is reported as SISH, but RetCCL and Yottixel also show high performance on LUAD retrieval. In organ search, only RetCCL was able to retrieve slides of lung origin, while Yottixel and SISH performed poorly, but for subtype retrieval, all three methods were able to correctly retrieve several slides of LUAD (Figure 2a).

3.2 Low Grade Glioma Slide Retrieval

For Low Grade Glioma (LGG) case, SISH is reported as the highest performing algorithm for retrieval by subtype search, though RetCCL and Yottixel also have significant performances. Only RetCCL correctly retrieves LGG slides on subtype search whereas both Yottixel and SISH retrieve Glioblastoma cases, and all three methods correctly retrieve slides containing brain tissue for organ retrieval (Figure 2b).

3.3 Hepatocellular Carcinoma Slide Retrieval

For Hepatocellular Carcinoma (LIHC) subtype retrieval, SISH, Yottixel, and RetCCL have comparable performance, but for liver organ search, RetCCL shows higher performance. Both Yottixel and SISH performed poorly on liver tissue retrieval, but RetCCL achieves perfect performance in identifying liver slides, while for subtype search, Yottixel and SISH retrieve correct LIHC cases but RetCCL mistakenly retrieves several cases of Cholangiocarcinoma (Figure 2c).

3.4 Patch Retrieval on Lung Adenocarcinoma

For identifying similar patches of interest in Lung Adenocarcinoma, RetCCL is the most consistent at retrieving patches of lung glandular cell, but all three models may have difficulties in discriminating more granular, subtle features of malignancy. When querying a patch containing normal alveolar tissue, all three models correctly retrieve patches corresponding to normal alveolar tissue, but some patches from SISH and Yottixel include thickened layers of fibroblasts, suggesting potential limitations in their ability to discriminate subtle differences (Figure 3).

4 Discussion

In this case study, we evaluated the performance and clinical utility of state-of-the-art histopathology slide search engines, Yotixxel, SISH, and RetCCL on real patient samples. While these models demonstrate significant advancements in the field, all exhibit certain shortcomings when trialing them on real patient cases deemed to be of moderate diagnostic difficulty by pathologists, indicating further progress is warranted.

We found that RetCCL was the most reliable in tissue retrieval by correctly identifying within the first five retrieved slides the correct tissue of diagnosis for all three cases. In contrast, both Yottixel and SISH failed to retrieve the correct tissue of origin at all top five ranked positions for two out of the three cases, which was unexpected given prior work demonstrating the high performance of these models.

For subtype search, we found overall higher performance amongst all three models than for tissue search, a discrepancy which has been reported previously. However, a significant component of this higher performance may be attributed to the narrowing of the search domain as all three subtype search methods require pre-selecting the tissue of interest. We also found that commonly used metrics in the literature for evaluation, such as mMW@5, may also be less clinically useful for real life scenarios. For example, while SISH subtype search on Slide 1 correctly retrieves a LUAD slide, when using the mMW@5 metric, this would still result in a perfect score of 100, despite the exclusion of the other 67 slides pertaining to LUAD in our dataset.

At the patch level, we find that RetCCL was more capable of identifying similar patches containing lung glandular cells but all three models struggled to differentiate between more subtle features of malignancy, such as the loss of cell borders and prominent nucleoli. These differences in performance may be attributed to RetCCL’s use of self-supervised learning for feature representation over the use of previous methods. Similarly, we also found that RetCCL outperformed both SISH and Yotixxel in retrieving patches containing normal alveolar tissue. Of note, the utility of these models in retrieving cancerous versus non-cancerous slides has yet to be formally investigated as these search engines were not intentionally designed for this task. Nevertheless, for search results to be accepted as reliably accurate by the clinical community, particularly on tasks such as patch-level retrieval where differences can be more pronounced, these capabilities may need to be eventually demonstrated as well.

As the field of digital pathology continues to evolve, we anticipate exciting developments in the near future. These will likely include more efficient and reliable systems for indexing and searching of

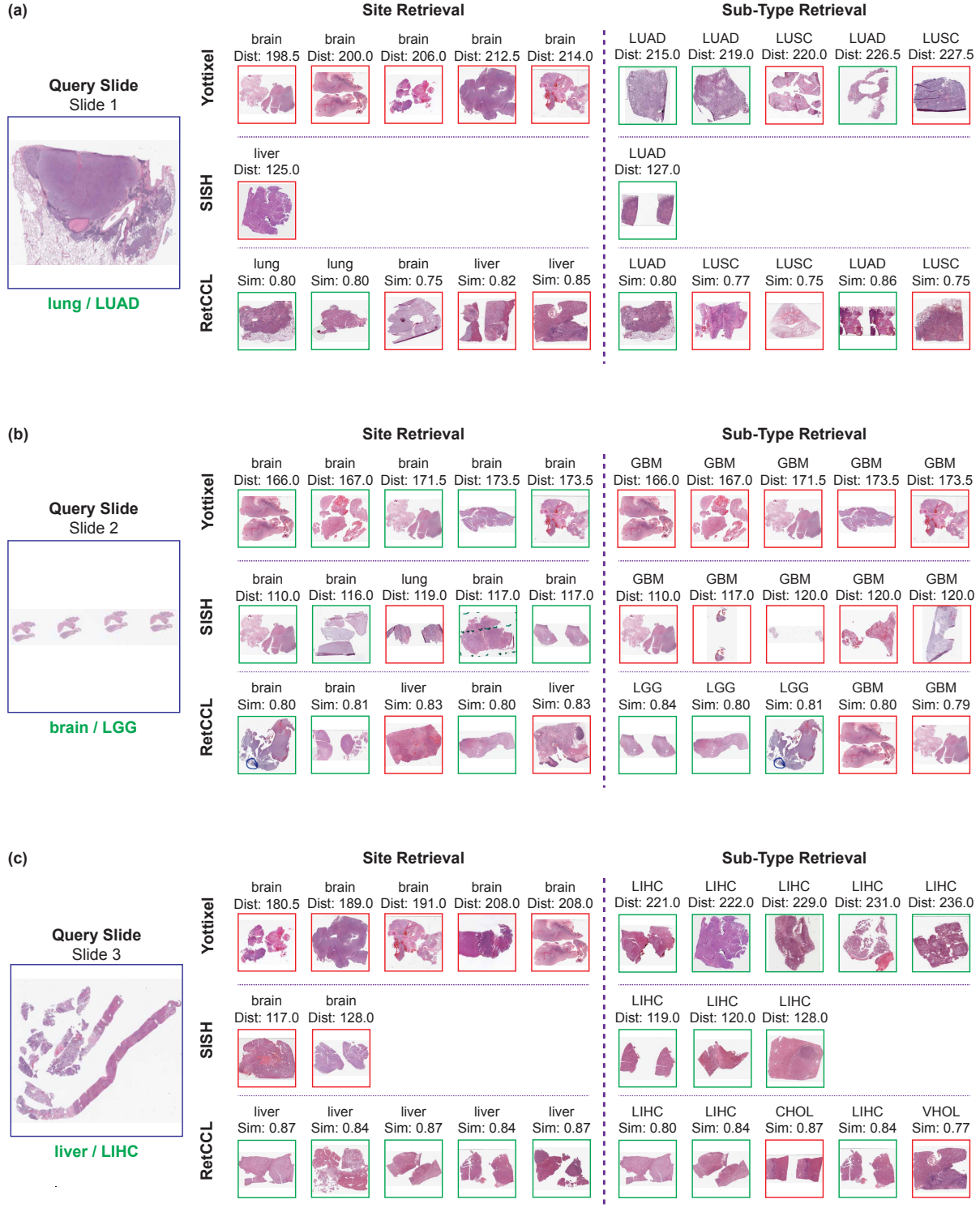


Figure 2: Results of site retrieval (left) and sub-type retrieval (right) at slide level for all three test slides. Correct labels are printed in green under query slides. Green border means correct label; red border means wrong label. For details about distances and similarities, see Section 2.1.

histopathology slides, increasingly robust algorithms for feature extraction, and potentially transformative diagnostic tools. However, given the high-stakes nature of patient care, we anticipate a significant amount of work ahead to ensure the validity and generalizability of these models prior to clinical adoption.

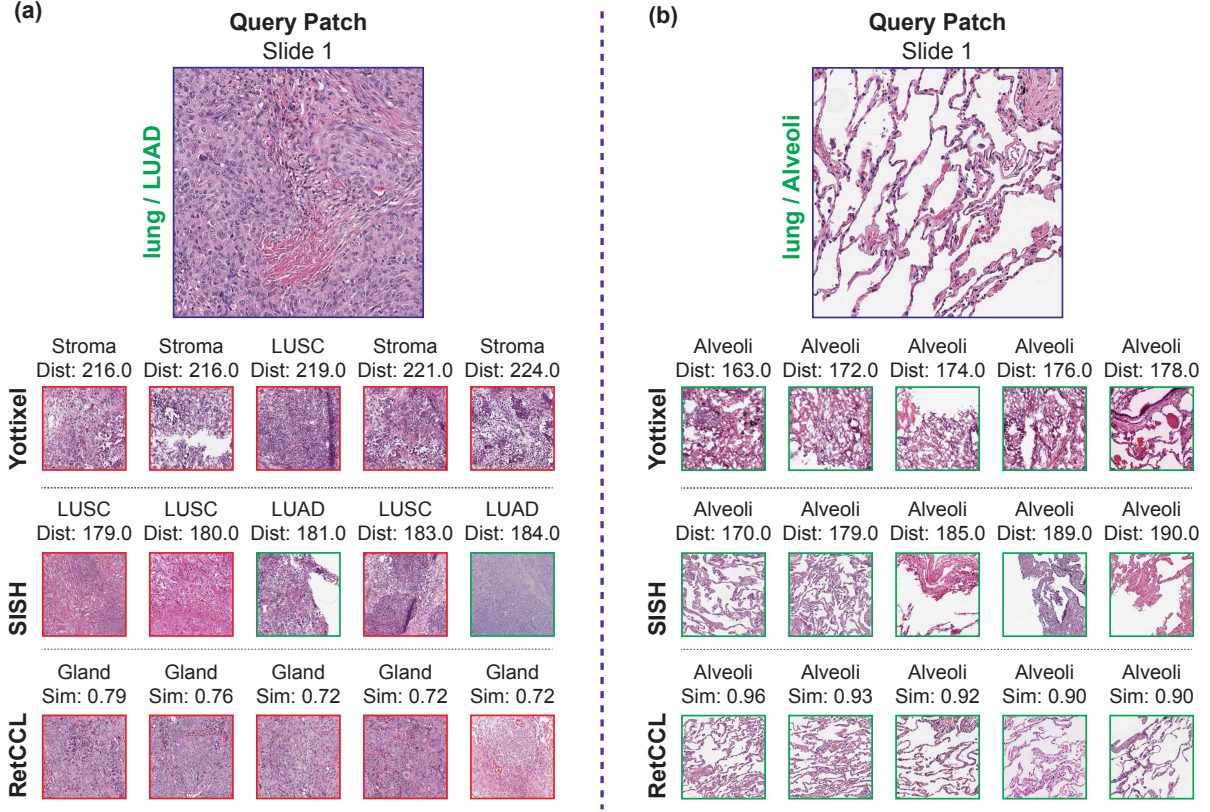


Figure 3: Results of patch retrieval for two patches from Slide 1. Correct labels are printed in green to the left of query patches. Green border means correct label; red border means wrong label. For details about distances and similarities, see Section 2.1.

To this end, we propose a framework of minimal requirements designed to facilitate the development of these systems in a manner that is both fair and transparent while minimizing patient harm and maximizing clinical utility:

1. **Open access to indexed databases and code:** Achieving clinical readiness for these systems demands the sharing of both model development code and indexed databases. This transparency not only fosters scientific integrity but also accelerates the pace of innovation through collective efforts.
2. **Replicability and generalizability of results across different health systems:** A vital measure of clinical applicability is the model’s performance across diverse clinical populations and environments, as in the case of real-world health systems.
3. **Clear explanation of algorithmic innovation and clinical benefit:** For clinical adoption, the unique aspects of each model and their direct value need to be clearly communicated. We propose the inclusion of two additional tasks where image search will be most helpful to pathologists in identifying the tissue of cancerous origin (in the metastatic setting) and distinguishing between cancerous and non-cancerous tissue.
4. **Fair and Balanced Comparison of Models:** Clinical adoption of these systems is contingent upon their measured performance relative to their peers. This requires fair and balanced comparisons using identical pre- and post-processing methods and the adoption of new metrics that accurately reflect clinical utility.
5. **Realistic and Transparent Discussion of Computational Efficiency:** Clinical applicability not only requires theoretical efficiency, but also hinges on the performance of these systems in a real-world, high-demand environment. Thus, discussions on computational efficiency should reflect the realities of clinical implementation.

As we continue to make strides in the development of histopathology slide search engines, it is imperative that we maintain a steadfast focus on these requirements. By doing so, we will ensure that these systems are not only theoretically sound, but also ready for meaningful clinical application.

Code and Data Availability

The test slides along with the updated source codes for all three methods used to generate the results can be found at github.com/jacobluber/PathologySearchComparison. All the data used in databases are publicly available at portal.gdc.cancer.gov. The list of data included in the database can also be found in the github repository above.

Funding

This work was supported by a University of Texas System Rising STARS Award (J.M.L) and the CPRIT First Time Faculty Award (J.M.L).

Competing Interests

No competing interests are disclosed by the authors.

References

- Chen, C., Lu, M. Y., Williamson, D. F. K., Chen, T. Y., Schaumberg, A. J., & Mahmood, F. (2022). Fast and scalable search of whole-slide images via self-supervised deep learning [Number: 12 Publisher: Nature Publishing Group]. *Nature Biomedical Engineering*, 6(12), 1420–1434. <https://doi.org/10.1038/s41551-022-00929-8>
- Gutman, D. A., Cobb, J., Somanna, D., Park, Y., Wang, F., Kurc, T., Saltz, J. H., Brat, D. J., & Cooper, L. A. D. (2013). Cancer Digital Slide Archive: An informatics resource to support integrated in silico analysis of TCGA pathology data. *Journal of the American Medical Informatics Association: JAMIA*, 20(6), 1091–1098. <https://doi.org/10.1136/amiajnl-2012-001469>
- Hamming, R. W. (1950). Error detecting and error correcting codes. *The Bell system technical journal*, 29(2), 147–160.
- Hegde, N., Hipp, J. D., Liu, Y., Emmert-Buck, M., Reif, E., Smilkov, D., Terry, M., Cai, C. J., Amin, M. B., Mermel, C. H., Nelson, P. Q., Peng, L. H., Corrado, G. S., & Stumpe, M. C. (2019). Similar image search for histopathology: SMILY [Number: 1 Publisher: Nature Publishing Group]. *npj Digital Medicine*, 2(1), 1–9. <https://doi.org/10.1038/s41746-019-0131-z>
- Kalra, S., Tizhoosh, H. R., Choi, C., Shah, S., Diamandis, P., Campbell, C. J. V., & Pantanowitz, L. (2020). Yottixel - An Image Search Engine for Large Archives of Histopathology Whole Slide Images. *Medical Image Analysis*, 65, 101757. <https://doi.org/10.1016/j.media.2020.101757>
- Kalra, S., Tizhoosh, H. R., Shah, S., Choi, C., Damaskinos, S., Safarpour, A., Shafiei, S., Babaie, M., Diamandis, P., Campbell, C. J. V., & Pantanowitz, L. (2020). Pan-cancer diagnostic consensus through searching archival histopathology images using artificial intelligence. *NPJ Digital Medicine*, 3, 31. <https://doi.org/10.1038/s41746-020-0238-2>
- Lew, M. S., Sebe, N., Djeraba, C., & Jain, R. (2006). Content-based multimedia information retrieval: State of the art and challenges. *ACM Transactions on Multimedia Computing, Communications, and Applications*, 2(1), 1–19. <https://doi.org/10.1145/1126004.1126005>
- Li, Z., Zhang, X., Müller, H., & Zhang, S. (2018). Large-scale retrieval for medical image analytics: A comprehensive review. *Medical Image Analysis*, 43, 66–84. <https://doi.org/10.1016/j.media.2017.09.007>
- Oord, A. v. d., Li, Y., & Vinyals, O. (2019). Representation Learning with Contrastive Predictive Coding [arXiv:1807.03748 [cs, stat]]. <https://doi.org/10.48550/arXiv.1807.03748>
- Oord, A. v. d., Vinyals, O., & Kavukcuoglu, K. (2018). Neural Discrete Representation Learning [arXiv:1711.00937 [cs]]. <https://doi.org/10.48550/arXiv.1711.00937>

- Riasatian, A., Babaie, M., Maleki, D., Kalra, S., Valipour, M., Hemati, S., Zaveri, M., Safarpour, A., Shafiei, S., Afshari, M., Rasoolijaberi, M., Sikaroudi, M., Adnan, M., Shah, S., Choi, C., Damaskinos, S., Campbell, C. J., Diamandis, P., Pantanowitz, L., . . . Tizhoosh, H. R. (2021). Fine-Tuning and Training of DenseNet for Histopathology Image Representation Using TCGA Diagnostic Slides [arXiv:2101.07903 [eess]]. <https://doi.org/10.48550/arXiv.2101.07903>
- Sikaroudi, M., Afshari, M., Shafique, A., Kalra, S., & Tizhoosh, H. R. (2023). Comments on 'fast and scalable search of whole-slide images via self-supervised deep learning'.
- Tizhoosh, H. R. (2015). Barcode annotations for medical image retrieval: A preliminary investigation. *2015 IEEE International Conference on Image Processing (ICIP)*, 818–822. <https://doi.org/10.1109/ICIP.2015.7350913>
- Tizhoosh, H. R., Zhu, S., Lo, H., Chaudhari, V., & Mehdi, T. (2016). MinMax Radon Barcodes for Medical Image Retrieval [arXiv:1610.00318 [cs]]. <https://doi.org/10.48550/arXiv.1610.00318>
- van Emde Boas, P. (1977). Preserving order in a forest in less than logarithmic time and linear space. *Information Processing Letters*, 6(3), 80–82. [https://doi.org/10.1016/0020-0190\(77\)90031-X](https://doi.org/10.1016/0020-0190(77)90031-X)
- Wang, X., Du, Y., Yang, S., Zhang, J., Wang, M., Zhang, J., Yang, W., Huang, J., & Han, X. (2023). RetCCL: Clustering-guided contrastive learning for whole-slide image retrieval. *Medical Image Analysis*, 83, 102645. <https://doi.org/10.1016/j.media.2022.102645>
- Weinstein, J. N., Collisson, E. A., Mills, G. B., Shaw, K. R. M., Ozenberger, B. A., Ellrott, K., Shmulevich, I., Sander, C., & Stuart, J. M. (2013). The Cancer Genome Atlas Pan-Cancer analysis project [Number: 10 Publisher: Nature Publishing Group]. *Nature Genetics*, 45(10), 1113–1120. <https://doi.org/10.1038/ng.2764>

Supplementary Material

Supplementary Methods

H&E Staining and Preparation

Tissues were stained with Harris’ hematoxylin solution for 6 h at a temperature of 60 °C–70 °C and were then rinsed in tap water until the water was colorless. Next, 10% acetic acid and 85% ethanol in water were used to differentiate the tissue 2 times for 2 h and 10 h, and the tissues were rinsed with tap water. In the bluing step, we soaked the tissue in saturated lithium carbonate solution for 12 h and then rinsed it with tap water. Finally, staining was performed with eosin Y ethanol solution for 48 h. Tissues were dehydrated with 95% ethanol twice for 0.5 h, and then soaked in xylene for 1 h at 60 °C–70 °C followed by paraffin for 12 h. The stained tissues were cut into 7 μ m slices, dewaxed, mounted with neutral balsam and then imaged using Nikon NIS-Elements microscopy.

Search Engines Used in Comparison

In the **Yottixel** method, the initial preprocessing step involves segmenting the foreground from the background in large whole slide images (WSIs). The segmented foreground is then divided into patches of size 1000 \times 1000 for 20 \times slides and 2000 \times 2000 for 40 \times slides. The 2000 \times 2000 patches are resized to 1000 \times 1000 before being input to the feature extractor. These patches undergo clustering using the K-means algorithm, resulting in 9 clusters based on the RGB histogram of each patch. A further selection process is applied, retaining 15% of the patches in each cluster using another K-means clustering method based on the spatial coordinates. This final collection of patches forms a ”mosaic.” The Yottixel model, as recommended by its authors (Kalra, Tizhoosh, Choi, et al., 2020), employs KimiaNet (Riasatian et al., 2021), a fine-tuned version of DenseNet specifically designed for histopathology slides, as the primary feature extractor (Fig. 1a). The outputs of the feature extractor undergo barcoding, where binary codes are generated from the extracted features. Thus, each WSI is represented by a set of barcodes (BoBs). The database comprises BoBs for each slide in the dataset. The distance between two BoBs is calculated as the median of the minimum Hamming distances (Hamming, 1950) between each barcode in the first BoB and all barcodes in the second BoB. When a query slide is introduced, it is converted into a BoB. The distance between the query BoB and all BoBs in the database is computed, and the top 5 slides with the lowest distances are returned. For patch retrieval, the query BoB is not required, and instead, the top 5 patches from all BoBs with the minimum distances to the query patch are retrieved.

The **SISH** method uses a similar approach to Yottixel for mosaic generation, with patch sizes of 1024 \times 1024 for 20 \times slides and 2048 \times 2048 for 40 \times slides. After mosaic generation, artifacts such as pure white patches are filtered out. The feature extraction in SISH consists of two parts: feature and index (Fig. 1b). The feature extraction process is the same as Yottixel, where each patch in the mosaic is fed into a pretrained DenseNet, and the resulting features are binarized. The index, however, is obtained from a pretrained VQ-VAE. The patch is encoded, resulting in a latent code, which is then subjected to three layers of average pooling. The output of these layers is multiplied by scaling factors, and the sum of these results represents the index in the VEB tree. This creates the database. When querying a slide, it is converted into a mosaic, and indices and features are generated from the patches in the query mosaic. The ”guided VEB search” algorithm is utilized, leveraging the properties of VEB trees, forward and backward searches, and entropy-based uncertainty calculations to retrieve the top slides based on hamming distance. The ranking algorithm accounts for class imbalance when returning the results. For patch retrieval, an index and feature are created for the query patch using a similar approach, and the best matches are found among the patches in the mosaics of the database. They also use a hamming distance threshold of 128 to make sure they only keep high quality results. That is why sometimes they return only a few matches.

RetCCL, drawing inspiration from both Yottixel and SISH, adopts a distinct approach. Instead of clustering patches based on RGB histogram values, RetCCL first obtains contrastive-based feature vectors for each patch within the segmented foreground tiles. These features serve as inputs for a 9-class K-means clustering. Within each cluster, an additional K-means process based on spatial coordinates is performed to select 20% of the patches. These selected patches form the mosaics, which constitute the database. The proposed feature extraction algorithm in RetCCL utilizes a clustering-guided contrastive learning method, employing the InfoNCE loss introduced in (Oord et al., 2019) (Fig. 1c). Given the

prevalence of normal cells in WSIs, learning irregularities from a limited number of patches becomes crucial. The self-supervised feature extractor employs two InfoNCE losses to capture irregular regions in patches.

For retrieving similar slides, a query slide is first transformed into a mosaic, generating a set of features for each patch in the mosaic. Similarity between two patches is measured using cosine similarity between their feature vectors. The retrieval process involves returning a set of patches in the database that exhibit a similarity score of at least 70% to the query patch. Each query patch and its corresponding results form a "bag." To account for class imbalance, an entropy-based uncertainty measure is calculated based on the occurrence of each label within the bag. Patch members in the bag are sorted according to this entropy measure. A threshold is then determined to remove lower quality results. Ultimately, the top 5 samples within each bag are returned as the final results for slide retrieval. For patch retrieval, only the top 5 patches with the highest cosine similarity scores are returned.

Supplementary Results

Lung Adenocarcinoma Slide Retrieval

Slide 1 is a Lung Adenocarcinoma (LUAD) case from a patient's partial lobectomy. The highest performing model in the literature on retrieving LUAD slides using subtype search is SISH; in their seminal paper, Chen et. al reported a mMV@5 (the mean average precision for the top 5 results) of 70-80 on retrieving LUAD from TCGA when applying subtype retrieval, which was maintained when testing against an independent test cohort of 1,377 LUAD slides. In contrast, the authors of RetCCL reported a mMV@5 of 84.01 relative to Yottixel's 70.96 on LUAD when applying subtype retrieval on 538 FFPE WSIs.

Amongst the three models tested, only RetCCL WSI organ search was able to retrieve slides that were of lung origin (Fig. 2a). Yottixel organ search only identifies slides pertaining to brain tissue, despite the presence of over 100 lung tissue slides in our dataset. We also found poor performance when using SISH organ retrieval as only one slide was retrieved corresponding to liver tissue. For subtype retrieval, we found that all three methods were now able to correctly retrieve several slides of LUAD in the top ranked position by subtype search. The extended results are provided in Supplementary Table 2.

Low Grade Glioma Slide Retrieval

We next investigated the performance of these algorithms on a Low Grade Glioma (LGG) case in Slide 2. This case was chosen given the known difficulty of differentiating Lower from Higher Grade Gliomas by morphology alone with molecular-based studies recently replacing histological classification as the gold standard for subtyping and grading.

The highest performing algorithm in the literature for LGG retrieval by subtype search is again SISH, which achieved a mMV@5 of nearly 100 when using the TCGA dataset's 838 LGG slides for subtype search, which is significantly higher from Yottixel's mMV@5 of 80-90. In contrast, the authors of RetCCL reported lower performance relative to Yottixel on LGG retrieval by subtype search on an independent cohort of 1699 brain FFPE WSIs, achieving a mMV@5 of 83.73 versus 89.77, respectively.

For Slide 2, we found that only RetCCL correctly retrieves LGG slides on subtype search whereas both Yottixel and SISH retrieve Glioblastoma (GBM) cases at all top five positions (Fig. 2b). For organ retrieval, Yottixel, SISH, and RetCCL all correctly retrieve slides containing brain tissue at top ranking positions with comparable performance. The extended results can be found in Supplementary Table 3.

Hepatocellular Carcinoma Slide Retrieval

Slide 3 is from a patient with Hepatocellular Carcinoma (LIHC) who underwent a liver biopsy by fine needle aspiration. Chen et. al previously demonstrated comparable performance on subtype retrieval for LIHC between SISH and Yottixel with a mMV@5 of 80-90 on the TCGA database. The authors of RetCCL also achieved similar performance as Yottixel across an independent cohort of 398 LIHC WSIs with a mMV@5 of 96.06 and 93.65, respectively. In regards to liver organ search, RetCCL has shown higher performance, achieving a mMV@10 of 89.97 versus 63.75 for Yottixel on 628 FFPE liver WSIs. In contrast, SISH and Yottixel achieved similar performance on liver tissue retrieval with a mMV@10 of 60-70 using TCGA.

As with lung tissue, we found poor performance for both Yotixxel and SISH on liver tissue retrieval as both queries resulted in brain slides only (Fig. 2c). We again find higher performance with RetCCL on organ search, which achieves perfect performance in identifying liver slides at all top five ranked positions. In contrast, for subtype search, we find higher performance for Yottixel and SISH, which now correctly only retrieve LIHC cases, whereas for RETTCL, several cases of Cholangiocarcinoma (CHOL) are mistakenly retrieved. The extended results are provided in Supplementary Table 4.

Patch Retrieval on Lung Adenocarcinoma

To better interpret granular differences in feature extraction, we next evaluated the performance of the three models on identifying similar patches of interest. For this task, we chose a patch from Slide 1 corresponding to an area of neoplastic LUAD cells with expected features of malignancy, such as abundant cytoplasm, nuclear crowding, loss of clear intracellular borders, and prominent nucleoli.

At the patch level, we find RetCCL is the most consistent at retrieving patches of lung glandular cell. However, these patches only contain normal glandular cells whereas in our queried patch, we have an abundance of neoplastic glandular cells, suggesting a weakness in discriminating more granular, cellular features of malignancy, which are subtle yet still discernible to pathologists. For Yottixel and SISH, we see less consistent retrieval of lung glandular tissue with several examples of primarily stroma and scant glandular cells as well as several examples of normal glandular tissue. As a whole, this suggests that RetCCL may have better performance in capturing higher-level features but all three models may have difficulties in discriminating more granular, subtle features of malignancy.

We also queried a patch containing normal alveolar tissue, which has more visually pronounced structural differences from glandular tissue, including a network of thin epithelial cell walls. We now find that all three models now correctly retrieve patches corresponding to normal alveolar tissue, although some patches from SISH and Yottixel include thickened layers of fibroblasts interspaced within the alveoli walls, which can be reactive in the setting of inflammation or malignancy. This is in contrast to queried slide where the alveoli walls only contain a single layer of flattened squamous epithelial cells, which can also be seen in the patches retrieved by RetCCL.

Unprocessed Slides

Supplementary Table 1: Unprocessed slides in the database for each model.

Model	Slide IDs
Yottixel	9ecf91d4-0d9e-4400-bf38-99420acd14cc
	f18b6fc0-6f40-4f0d-82ef-0b092a21b6bf
	846087b8-f70c-4970-a1b7-24d403229801
	c95681f3-53d4-4b15-833d-ff68f171965e
	71dc7ba0-a623-4aaf-9502-f2fe9d188401
	dc5d0b4-04ff-4731-bda1-8ad7cd0fa345
SISH	2dc5d0b4-04ff-4731-bda1-8ad7cd0fa345
RetCCL	All slides in the database processed.

Extended Results

Supplementary Table 2: Lung Adenocarcinoma Slide Retrieval

Rank	Yottixel Site	Yottixel Subtype	SISH Site	SISH Sub-type	RetCCL WSI Site	RetCCL Subtype
1	Brain (198.5)	Lung adeno-carcinoma (215.0)	Liver (125.0)	Lung adeno-carcinoma (127.0)	Lung (0.80)	Lung adeno-carcinoma (0.80)
2	Brain (200.0)	Lung adeno-carcinoma (218.5)	-	-	Lung (0.80)	Lung squamous cell carcinoma (0.77)
3	Brain (206.0)	Lung squamous cell carcinoma (220.0)	-	-	Brain (0.75)	Lung squamous cell carcinoma (0.75)
4	Brain (212.5)	Lung adeno-carcinoma (227.0)	-	-	Liver (0.82)	Lung adeno-carcinoma (0.86)
5	Brain (214.0)	Lung squamous cell carcinoma (227.5)	-	-	Liver (0.85)	Lung squamous cell carcinoma (0.75)

Supplementary Table 3: Low Grade Glioma Slide Retrieval

Rank	Yottixel Site	Yottixel Subtype	SISH Site	SISH Sub-type	RetCCL WSI Site	RetCCL Subtype
1	Brain (166.0)	Glioblastoma (166.0)	Brain (110.0)	Glioblastoma	Brain (0.80)	Lower Grade Glioma (0.84)
2	Brain (167.0)	Glioblastoma (167.0)	Brain (116.0)	Glioblastoma	Brain (0.81)	Lower Grade Glioma (0.80)
3	Brain (171.5)	Glioblastoma (171.5)	Lung (119.0)	Glioblastoma	Liver (0.83)	Lower Grade Glioma (0.81)
4	Brain (173.5)	Glioblastoma (173.5)	Brain (117.0)	Glioblastoma	Brain (0.80)	Lower Grade Glioma (0.80)
5	Brain (173.5)	Glioblastoma (173.5)	Brain (117.0)	Glioblastoma	Liver (0.83)	Lower Grade Glioma (0.79)

Supplementary Table 4: Hepatocellular Carcinoma Slide Retrieval

Rank	Yottixel Site	Yottixel Subtype	SISH Site	SISH Sub-type	RetCCL WSI Site	RetCCL Subtype
1	Brain (180.0)	Hepatocellular carcinoma (221.0)	Brain (117.0)	Hepatocellular carcinoma (119.0)	Liver (0.87)	Hepatocellular carcinoma (0.80)
2	Brain (189.0)	Hepatocellular carcinoma (222.0)	Brain (128.0)	Hepatocellular carcinoma (120.0)	Liver (0.84)	Hepatocellular carcinoma (0.84)
3	Brain (191.0)	Hepatocellular carcinoma (229.0)	-	Hepatocellular carcinoma (128.0)	Liver (0.87)	Cholangiocarcinoma (0.87)
4	Brain (208.0)	Hepatocellular carcinoma (231.0)	-	-	Liver (0.84)	Hepatocellular carcinoma (0.84)
5	Brain (208.0)	Hepatocellular carcinoma (236.0)	-	-	Liver (0.87)	Cholangiocarcinoma (0.77)